

FERROMAGNETIC INCLUSIONS IN GEOMATERIALS: IMPLICATIONS

By Katherine Klein¹ and J. Carlos Santamarina²

ABSTRACT: Various laboratory and field techniques used to study geomaterials utilize the principles of electromagnetism. Applications in geotechnical engineering such as resistivity profiling, induced polarization, ground-penetrating radar, and time-domain reflectometry, focus on the electrical properties of the materials and neglect the magnetic component. Yet the a priori assumption that the medium is nonferromagnetic may lead to significant errors in data interpretation because the presence of ferromagnetic materials affects the propagation of electromagnetic waves. An experimental study is conducted using kaolinite with ferromagnetic inclusions. Results show that magnetic permeability is a function of the volume fraction and spatial distribution of ferromagnetic inclusions; the interaction among inclusions increases with increasing volume fraction and proximity. These results and published data show that a relaxation due to "wall bowing" occurs at kilohertz frequencies, and a relaxation due to "wall displacement" occurs at megahertz frequencies. It is shown that the relative permittivity (real and imaginary components) inferred from wave-propagation measurements is larger than the actual value by a factor approximately equal to the real relative magnetic permeability. Corrections for ferromagnetic effects must be computed using parameters measured at the same frequency.

INTRODUCTION

Electromagnetic waves have been used to study the behavior of geomaterials for more than a century. These techniques measure the response of charges within a material to an electromagnetic perturbation. The frequency and wavelength of the applied field can vary over many orders of magnitude, thereby enabling the study of many different time and spatial scales within the material. It follows from Maxwell's equations that three material parameters are needed to describe interactions between electromagnetic waves and the medium: electrical conductivity σ , complex dielectric permittivity κ^* , and complex magnetic permeability μ^* .

Several field methods based on electromagnetic principles are used to obtain information about stratigraphy, location of anomalies (e.g., water table, metallic objects, cavities, and contaminants), and soil properties (e.g., porosity, structure, and pore fluid). Field techniques include resistivity profiling [e.g., Ward (1990)], magnetometric resistivity [e.g., Edwards and Nabighian (1991)], induced polarization [e.g., Marshall and Madden (1959)], ground penetrating radar [e.g., Daniels and Roberts (1994)], and time-domain reflectometry [e.g., Topp et al. (1984)].

On the other hand, laboratory measurements are conducted to characterize materials in view of site exploration, to enhance the understanding of geomaterials (e.g., water content, anisotropy, and interactions in soil-water-electrolyte-chemical systems), or to gain insight into geoprocesses (e.g., consolidation/sedimentation, chemical diffusion, corrosion, and hardening of soil-cement slurries). Conductivity and permittivity are measured using four-electrode systems (transfer function approach analysis), two-electrode systems (equivalent circuits analysis), or transmission line techniques (wave-propagation analysis). The four-electrode and two-electrode methods are applicable at hertz-to-megahertz frequencies, and transmission line methods operate at megahertz-to-gigahertz frequencies (Klein and Santamarina 1997).

Explicit magnetic permeability/susceptibility measurements

¹Asst. Prof., Univ. of Toronto, Toronto, ON, Canada; formerly, Grad. Student, Georgia Inst. of Technol., Atlanta, GA 30332.

²Prof., School of Civ. and Envir. Engrg., Georgia Inst. of Technol., Atlanta, GA.

Note. Discussion open until July 1, 2000. To extend the closing date one month, a written request must be filed with the ASCE Manager of Journals. The manuscript for this paper was submitted for review and possible publication on March 11, 1999. This paper is part of the *Journal of Geotechnical and Geoenvironmental Engineering*, Vol. 126, No. 2, February, 2000. ©ASCE, ISSN 1090-0241/00/0002-0167-0179/\$8.00 + \$.50 per page. Paper No. 20412.

of geomaterials have been performed both in the laboratory and in the field for various reasons, including to assess soil uniformity, determine geochemical characteristics and stratigraphy of loess, detect hydrocarbon deposits, and find archeological remains. In addition to these specific applications, most field and laboratory studies based on electromagnetic principles assume that the magnetic permeability of the specimen is negligible. Because the presence of ferromagnetic inclusions affects the propagation of electromagnetic waves, significant errors can develop in the analysis of data should the nonferromagnetic assumption not apply. Therefore, before interpreting field or laboratory data, this assumption must be verified.

The objectives of this study are to review the magnetic properties of geomaterials, to use simple measurement and analysis procedures to assess the magnetic permeability of various soil specimens, to determine the effect of quantity and spatial distribution of ferromagnetic inclusions on the magnetic permeability of soil specimens, and to examine the effect of ferromagnetic impurities on permittivity measurements and wave parameters used in field studies.

MAGNETIC PROPERTIES OF GEOMATERIALS

The ability of a material to be magnetized is characterized by the magnetic permeability μ^* , which is determined from magnetization curves [i.e., the variation in the magnetic induction B (Wb/m²) with the applied field H (A/m)]

$$B = \mu_0(H + M) \quad (1)$$

where M = magnetization of the specimen (A/m); and μ_0 = magnetic permeability of vacuum ($4\pi \cdot 10^{-7}$ H/m). In the case of a linear magnetic material, M is directly proportional to H

$$M = \chi^*H \quad (2)$$

where $\chi^* = \chi' - j\chi''$ = complex magnetic susceptibility (dimensionless) consisting of real χ' and imaginary χ'' components [asterisk (*) denotes a complex quantity]. Eq. (1) becomes

$$B = \mu_0(1 + \chi^*)H = \mu^*H = \mu_0\mu_{rel}^*H \quad (3)$$

where $\mu_{rel}^* = 1 + \chi^* = \mu'_{rel} - j\mu''_{rel}$ = magnetic permeability of the material normalized with respect to the permeability of free space, $\mu_0 = 4\pi \cdot 10^{-7}$ H/m. The real part of the relative permeability μ'_{rel} represents the magnetizability of the material, and the imaginary part μ''_{rel} represents energy losses. Based on

thermodynamic relationships, the real relative permeability must be greater than zero or $\chi' > -1$ (Landau et al. 1984).

Magnetization Mechanisms

Magnetic fields develop through the movement of charges. Because matter consists of charged particles (electrons and protons), it exhibits magnetic properties. Magnetism arises due to the partial filling of electron shells resulting in unpaired electrons (i.e., uncompensated charges). The distribution of the electrons in an iron atom is presented in Table 1. In all the shells, except for the 3*d* shell, the positive spin electrons compensate the magnetic moments generated by the negative spin electrons, and the shells do not carry a magnetic charge. However, in the 3*d* shell, the positive magnetic moments are not counteracted by negative magnetic moments resulting in a permanent magnetic moment. The contribution of the spin angular momentum v_s to the magnetization of a specimen is

$$v_s = -2m_s v_B \quad (4)$$

where v_B = Bohr magneton [9.274×10^{-24} J/T]; and m_s = spin quantum number.

The orbital motions of the electrons also contribute to the magnetic moment. The orbital angular momentum in a free atom is

$$v_l = -m_l v_B \quad (5)$$

where m_l = magnetic quantum number. However, electron orbits in solid matter are firmly fixed and are little influenced by an external magnetic field (Bozorth 1951). In fact, the contribution of the spin angular momentum to the magnetization of a solid is twice that of the orbital angular momentum (Halliday and Resnick 1988).

Diamagnetism and Paramagnetism

Diamagnetic materials (e.g., pure kaolinite and quartz) do not have permanent magnetic moments. Yet the altered orbital motion of electrons in the presence of a magnetic field produces a magnetic dipole moment that is proportional to the applied field but in the opposite direction. This induced dipole moment creates a small negative susceptibility; therefore, μ'_{rel} is slightly <1 [(3)].

Paramagnetic materials (e.g., montmorillonite and granite) have permanent dipole moments caused by the spin of electrons. In the absence of an external magnetic field, thermal agitation ensures that the magnetic dipoles are randomly oriented; thus, there is no resultant magnetization. However, in the presence of an applied external field, the magnetic dipoles orient parallel to the field, resulting in a slight net magnetization. The relative magnetic permeability of paramagnetic materials is slightly >1 . In general, the induced magnetization in paramagnetic and diamagnetic materials is proportional to the applied field, resulting in permeability/susceptibility values

TABLE 1. Distribution of Electrons in Iron Atom (Bozorth 1951)

Shell (1)	Total number of electrons (2)	Number of electrons with + spin (3)	Number of electrons with - spin (4)
1s	2	1	1
2s	2	1	1
2p	6	3	3
3s	2	1	1
3p	6	3	3
3d	6	5	1
4s	2	1	1

that are independent of field strength (Bleaney and Bleaney 1976). Table 2 summarizes magnetic permeability data for various geomaterials.

Ferromagnetism

In ferromagnetic materials (e.g., iron and nickel), the permanent dipole moments form "domains" where the magnetic dipoles are aligned in the same direction. In an unmagnetized state, domain directions are such that the net magnetization of the specimen is zero. The directions of domain magnetization are affected by crystal structure and/or by strain. In the case of an iron crystal without an applied magnetic field, the direction of easy magnetization is parallel to one of the crystal axes as shown in Fig. 1. A demagnetized crystal normally has 1/6 of its domains oriented in each of these directions of easy magnetization (Bozorth 1951). The direction of magnetization gradually rotates from one direction to the other at the boundaries between domains; Fig. 2 presents a schematic representation of the transition between domains (domain walls). The size of the domains depends on the size, shape, and magnet-

TABLE 2. Real Relative Magnetic Permeability of Various Materials

Material (1)	Real relative magnetic permeability μ'_{rel} (2)
Water ^a	0.9999100
Gold ^b	0.9999973
Silver ^b	0.9999981
Copper ^a	0.999990
Quartz (SiO ₂) ^b	0.999999 to 0.9999988
Kaolinite ^{cl} -mass susceptibility ^d	0.9999995 to 1.0000023
Montmorillonite (2.8% FeO, 3% Fe ₂ O ₃) ^b	1.000026
Illite (1.4% FeO, 4.7% Fe ₂ O ₃) ^b	1.000034
Shale ^b	1.000005 to 1.0015
Granite ^b	1 to 1.004
Ochre (hematite) ^c	1.002 to 1.003
Annealed nickel ^f	≈300 (initial-low H)
Laboratory iron ^f	≈550 (initial-low H)

^aOmar (1975).

^bCarmichael (1989).

^cSchroeder et al. (1998).

^dMass susceptibility = χ' /density of specimen (cm³/g).

^eThis study (frequency = 2 kHz).

^fBozorth (1951).

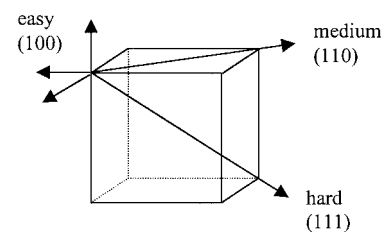


FIG. 1. Schematic Representation of Crystal Structure of Iron. Directions of Easy, Medium, and Hard Magnetization Are Shown (Bozorth 1951)

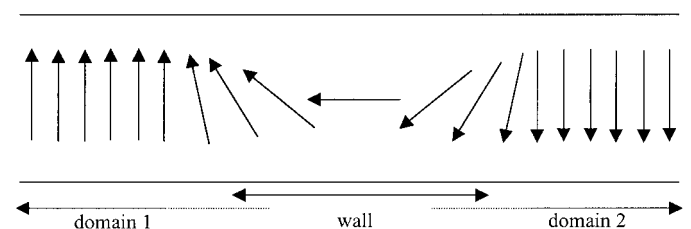


FIG. 2. Schematic Representation of Transition between Domains

ization history of the crystal, and it can vary between 10^{-3} and 1 mm^3 in volume. Particles with diameters less than about $1 \mu\text{m}$ consist of single domains (Bleaney and Bleaney 1976).

The magnetization of ferromagnetic materials through the application of a magnetic field occurs because of the rotation of the spins within the domains [Fig. 3(b)] or the movement of domain walls [Fig. 3(c)]. Fig. 4 shows a schematic representation of a magnetization curve and the associated magnetization mechanisms. Small magnetic fields have little effect on the direction of the spins within the domains but can affect the spins in the domain walls. At fields less than the threshold or critical field ($H < H_{cr}$), there is a net magnetization caused by the domain wall "bowing" or "bulging," and the pinned walls bend like flexible membranes owing to the applied magnetic field. This movement is reversible, and the permeability increases linearly with increasing H .

Once the applied field is greater than the critical field, wall unpinning, displacement, and repinning occur causing a large increase in magnetic permeability. The processes are irreversible. The critical field is dependent upon sample defects such as point defects, dislocations, other phases, and porosity,

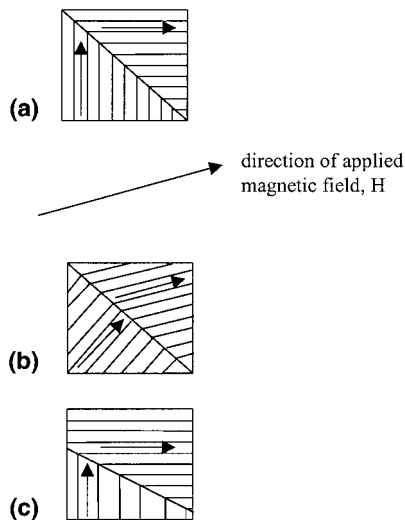


FIG. 3. Magnetization Mechanisms: (a) No Magnetic Field; (b) Rotation of Spins within Domains; (c) Movement of Domain Walls (Bozorth 1951)

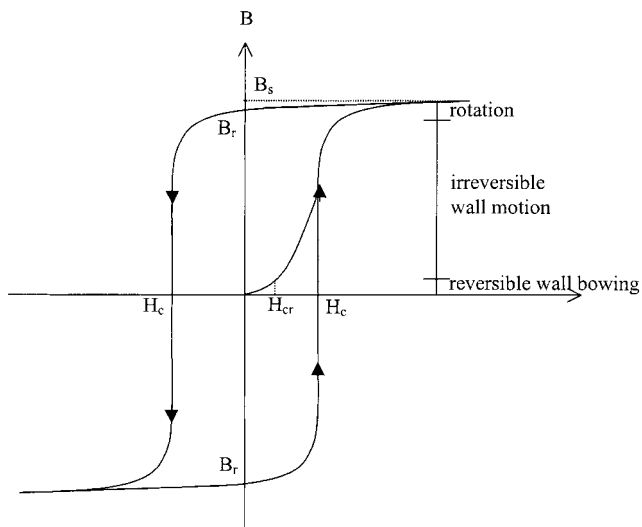


FIG. 4. Schematic Representation of Hysteresis Loop Where B Is Magnetic Induction That Remains upon Removal of Field after Saturating Specimen (Remanent Magnetic Induction); B_s = Saturation Magnetic Induction; H_c = Magnetic Field Required to Reach Zero Magnetic Induction (Coercivity)

which act as pinning sites. When the wall is displaced, it is pinned in a new position upon removal of the field; a larger field is required to cause additional movement (Valenzuela 1994).

Continued increase in the applied field causes the spins within the domains to rotate, resulting in saturation of the specimen; that is, the sample is a single domain oriented parallel to the applied field. Within this range of applied fields H , this mechanism is reversible, and permeability varies linearly with the applied field (Bleaney and Bleaney 1976).

Decreasing the field to zero after saturating the specimen does not result in zero magnetic induction but in a remanent state B_r . This hysteresis is due to the irreversible wall movements. The magnetic field required to reach zero magnetic induction is called the coercive force or coercivity H_c . When $H > H_c$, the magnetization reverses, and there is a tendency to saturate in the new direction. Upon removal of the field, there is a symmetric remanent magnetism B_r (Bleaney and Bleaney 1976).

The real relative permeability of ferromagnetic materials is >1 and is highly dependent upon the strength of the applied field, as indicated in Fig. 4.

Frequency Dependence of Magnetic Permeability

The magnetic permeability of a material varies with the frequency of the applied magnetic field. High frequency resonance (GHz) develops due to electron spins. In ferromagnetic materials, the magnetic moments in the domain walls are unable to follow the field at these high frequencies, and the only magnetization mechanism is the spin rotation in domains. When an external field is applied in a direction other than the spins' easy direction, the spins precess around the field direction for a certain time before reaching the new orientation (Valenzuela 1994).

Low frequency relaxations in ferromagnetic materials arise as a result of the movement of the domain walls (wall bowing and displacement). It follows from the previous discussion that the low frequency dispersions are dependent upon the applied magnetic field and the properties of the specimen. Fig. 5 shows the effect of field intensity H on the permeability spectrum. For $H < H_{cr}$, only wall bowing effects can be seen; for $H > H_{cr}$, the effects of both wall bowing and wall displacement are evident. Relaxations due to wall displacement occur at lower frequencies than wall bowing because wall displacement requires more time for unpinning, displacement, and repinning.

Fig. 6 exhibits the dependence of the low frequency permeability and the relaxation frequency on grain size. For a pinned wall, the initial permeability increases, and the relaxation frequency decreases as grain size increases. The relaxa-

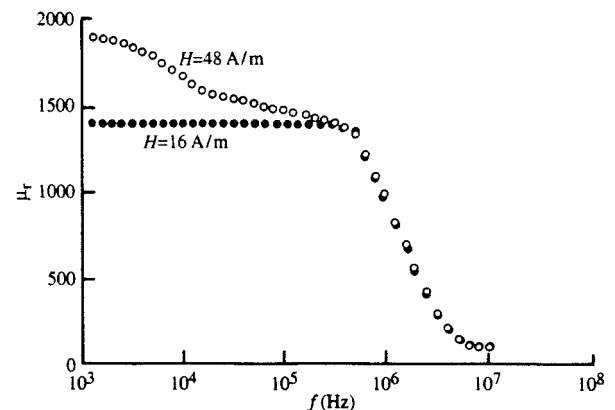


FIG. 5. Real Relative Magnetic Permeability Spectrum above Critical Magnetic Field H_{cr} (○) and below Critical Magnetic Field H_{cr} (●) for Ni-Zn Specimen (Valenzuela 1994)

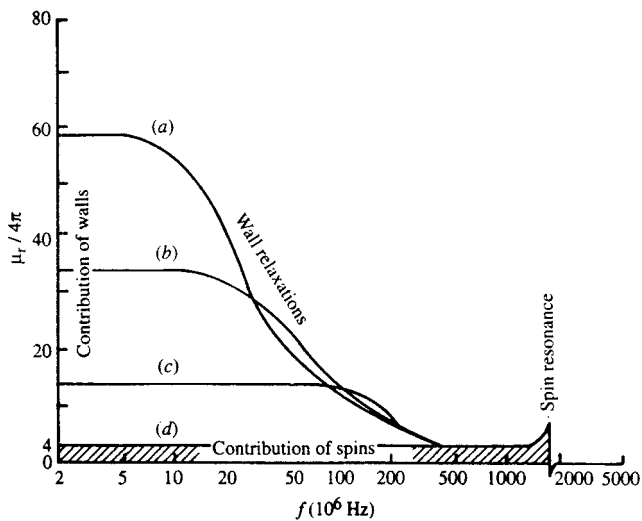


FIG. 6. Real Relative Magnetic Permeability Spectra of NiFe₂O₄ Specimens with Various Grain Sizes: (a) 11 μm; (b) 5 μm; (c) 2 μm; (d) <0.2 μm [Globus (1962) from Valenzuela (1994)]

tion frequency of the specimen increases as the insulation between particles increases, thereby reducing losses as a result of eddy currents (Gelinas et al. 1997).

Magnetization of Multiphase Media: Mixture Models

The permeability and the shape of the magnetization curve for a composite is dependent upon particle size distribution, particle shape, particle orientation, and the stress applied during specimen preparation (Adler et al. 1989). Table 3 presents various mixture models that describe the magnetic permeability of a medium with ferromagnetic inclusions in a nonconducting host medium.

The simple mixture model presented by Wagner considers that the magnetic susceptibility of a sphere placed in a uniform magnetic field is $\chi' = 3$ (Bleaney and Bleaney 1976; Gokturk et al. 1993). If particles do not interact (i.e., $v_2 < 0.2$ and particles are homogeneously distributed), the initial magnetic permeability increases linearly with the amount of ferromagnetic inclusions. At high volume fractions, interactions among particles act to increase the mixture magnetic permeability/susceptibility. As Wagner's model assumes no interactions, it provides a lower bound for the magnetic permeability of mixtures of ferromagnetic inclusions in a nonconducting host medium. Additional models exist that predict upper-bound permeability values [e.g., Hashin and Shtrikman (1962)].

TABLE 3. Magnetic Permeability Models for Ferromagnetic-Dielectric Mixtures

Model (1)	Equation (2)	Comments (3)
Wagner ^a	$\mu'_{\text{mix}} = \mu_0(1 + 3v_2)$	Spherical particles; $v_2 < 0.2$
Poisson ^b	$\mu_{\text{mix}} = \mu_1 \frac{[(\mu_2 + 2\mu_1)(\mu_1 - \mu_2)^{-1}] - 2v_2}{[(\mu_2 + 2\mu_1)(\mu_1 - \mu_2)^{-1}] + v_2}$	Conducting spheres in cubic array; moderate v_2
Doyle ^b	$\mu_{\text{mix}} = \mu_1 \frac{\left[\frac{(\mu_2 + 2\mu_1)}{(\mu_1 - \mu_2)} - 2v_2 + 1.305 \frac{(\mu_2 - \mu_1)}{(\mu_2 + 4\mu_1/3)} v_2^{10/3} \right]}{\left[\frac{(\mu_2 + 2\mu_1)}{(\mu_1 - \mu_2)} + v_2 + 1.305 \frac{(\mu_2 - \mu_1)}{(\mu_2 + 4\mu_1/3)} v_2^{10/3} \right]}$	Conducting spheres in simple cubic array; $v_2 < 0.67$

Note: μ_0 , μ_{mix} , μ_1 , and μ_2 = magnetic permeability of vacuum ($4\pi \cdot 10^7$ H/m), mixture, host medium, and inclusions, respectively; and v_2 = volume fraction of ferromagnetic inclusions.

^aGokturk et al. (1993).

^bDoyle (1978).

Measurement Techniques

There are many different techniques to measure the magnetic susceptibility or permeability of materials including force, change-in-flux, and transmission/reflection methods. Although magnetic susceptibility and permeability are complex quantities, only the real component is often measured. Fig. 7 presents schematic representations of the measurement techniques and summarizes the advantages and disadvantages of the methods.

EXPERIMENTAL STUDY: PROCEDURE

A series of tests was conducted to assess the effect of ferromagnetic inclusions in a nonferromagnetic soil host in response to an applied magnetic field. This section describes equipment, calibration, and data reduction procedures.

Equipment

Magnetic permeability values were determined by measuring the magnitude of impedance $|Z|$ and phase angle θ of specimens placed within a solenoid. From these values, the inductance L and resistance R of the system were determined as a function of frequency ($Z^* = R + j\omega L$). The measurements were performed using an HP-4192A Hewlett Packard low frequency impedance analyzer over the frequency range of 5 to 13 MHz. An HP-16047A test fixture connected the solenoid to the analyzer. This analyzer operates by applying a constant voltage V to the specimen at all frequencies. Because Z^* depends on frequency $Z^* = R + j\omega L = V/i$, the applied current i varies as a function of frequency. Thus, the magnetic induction B is also dependent on frequency as it is related to current by

$$B = \frac{\mu_0 i N}{l} \quad (6)$$

where μ_0 = permeability of vacuum; N = number of turns in the solenoid; and l = length of the solenoid. Fig. 8 shows the computed variation in B with frequency for a solenoid in air and for a solenoid filled with 100% iron filings (by weight). Figs. 9(a and b) show measured inductance and resistance values, respectively, for two tests conducted on a specimen of 100% iron filings. One test was performed keeping B constant (varying the applied voltage V), and the second test was conducted allowing B to vary as a function of frequency (keeping the applied voltage V constant). Fig. 9 shows that the measured inductance and resistance are independent of the magnetic induction for this specimen. Therefore, the magnetic permeability of the tested specimens are not a function of the applied magnetic induction for the low values of B imposed on the specimens $B < 3 \times 10^{-5}$ Wb/m² (Fig. 4).

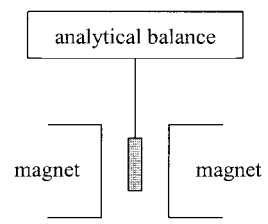
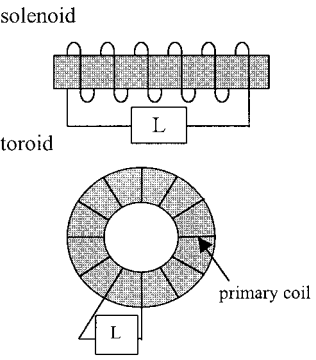
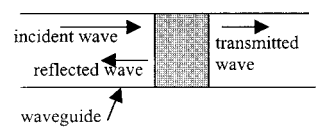
method	properties
Force Methods (Mulay, 1972) 	Gouy (non-uniform field) <i>permeability:</i> diamagnetic and paramagnetic <i>specimens:</i> powders or liquids <i>disadvantages:</i> large specimens, requires uniform specimen density, problems with magnetic anisotropy Faraday (uniform field) <i>permeability:</i> diamagnetic, paramagnetic, and ferromagnetic <i>specimens:</i> tablets <i>advantages:</i> high accuracy, small specimens, no packing errors <i>disadvantages:</i> problems with liquids, not applicable for magnetic anisotropy
Change-in-Flux Methods (Mulay, 1972; Hatfield, 1987) 	<i>permeability:</i> diamagnetic, paramagnetic, and ferromagnetic (requires external field) <i>specimens:</i> solids, powders, and liquids <i>frequency:</i> Hz to MHz <i>advantages:</i> no cumbersome force measurements, spectral response <i>disadvantages:</i> requires well-machined specimens if solid material, boundary effects in the case of the solenoid <i>analysis:</i> equivalent circuit Note: a secondary coil and an ammeter can be used instead of an impedance analyzer for measurements with toroids (Rowland ring).
Transmission/Reflection Methods (Baker-Jarvis et al., 1993) 	<i>permeability:</i> diamagnetic, paramagnetic, and ferromagnetic <i>specimens:</i> solids <i>frequency:</i> GHz <i>advantages:</i> easy to use, accurate, spectral response, permits study of anisotropy <i>disadvantages:</i> air gaps, resonance, may require well-machined specimens <i>analysis:</i> wave propagation

FIG. 7. Summary of Measurement Technique (Note: Specimen Is Shaded)

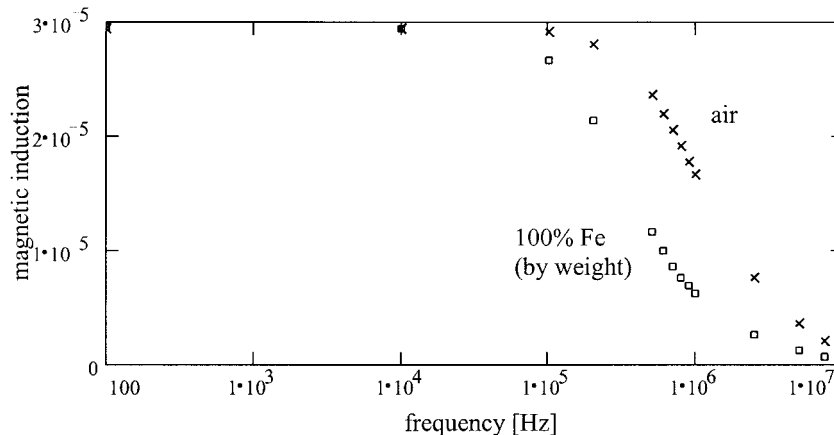


FIG. 8. Variation in Magnetic Induction B (Wb/m^2) as Function of Frequency for Specimens of Air and 100% Iron Filings (by Weight). Current Was Measured, and B Was Computed Using Eq. (6)

Data Reduction

The computation of the magnetic permeability from measured impedance values using a solenoid is based on equivalent circuit elements and considers a resistor R_{coil} in series with an inductor L . The measured impedance of this system is

$$Z^* = R_{\text{coil}} + j\omega L \quad (7)$$

where R_{coil} = resistance of the solenoid. The inductance in the solenoid is proportional to the magnetic permeability μ_{rel}^* of the specimen

$$L = \mu_{\text{rel}}^* L_0 = (\mu'_{\text{rel}} - j\mu''_{\text{rel}}) L_0 \quad (8)$$

where L_0 = inductance of the solenoid in vacuum, and it is a function of the cross-sectional area A , number of turns N , and the length l of the coil

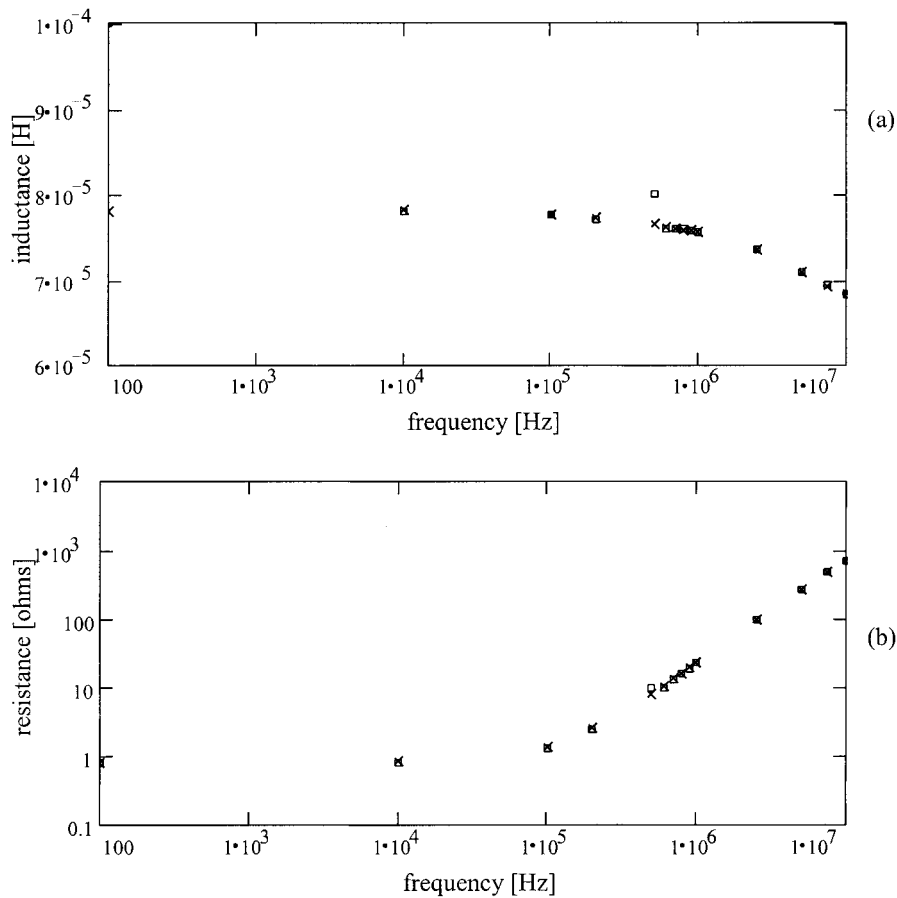


FIG. 9. Effect of Magnetic Induction B on Measurements in Solenoid: (a) Inductance; (b) Resistance. Tests Were Conducted on Specimen of 100% Iron Filings with Constant B (\square) and Varying B (\times)

$$L_0 = \mu_0 \frac{AN^2}{l} \quad (9)$$

Substituting (8) into (7)

$$Z' + jZ'' = (R_{\text{coil}} + \omega L_0 \mu''_{\text{rel}}) + j\omega \mu'_{\text{rel}} L_0 \quad (10)$$

Equating real and imaginary components and taking into consideration (9)

$$\mu'_{\text{rel}} = \frac{Z''}{\omega L_0} = \frac{Z'' l}{\omega AN^2 \mu_0} \quad (11)$$

$$\mu''_{\text{rel}} = \frac{Z' - R_{\text{coil}}}{\omega L_0} = \frac{(Z' - R_{\text{coil}}) l}{\omega AN^2 \mu_0} \quad (12)$$

Calibration

The calibration of the solenoid for magnetic permeability measurements involves the following four factors: solenoid geometry, resistance in the coil, residual and stray parameters, and incomplete coverage (discussed below).

Solenoid Geometry

Three solenoids with different geometrical characteristics were used to measure the magnetic permeability of air (Table 4). Following Welsby (1950), a correction for geometric effects was implemented

$$L_{\text{corr}} = L \cdot K \quad (13)$$

$$K = \left[1 + 0.9 \left(\frac{r}{l} \right) - 0.02 \left(\frac{r}{l} \right)^2 \right]^{-1} \quad (14)$$

where r = radius of the inductor; and l = length of the inductor.

TABLE 4. Solenoid Characteristics and Magnetic Permeability Measurements of Air

Number of turns N (1)	Length/diameter ratio (2)	μ'_{rel} of air (uncorrected) (3)	μ'_{rel} of air (corrected) (4)	Error ($\pm\%$) (5)
157	8	1.089	1.034	3.4
180	9.8	1.043	0.997	0.3
491	24	1.125	1.104	10.4

Fig. 10 shows the corrected and uncorrected real relative permeability measurements. The solenoid that resulted in data closest to the theoretical value of air, $\mu'_{\text{rel}} = 1$, was the solenoid with $l = 7.4$ cm, $A = 0.449$ cm², and $N = 180$. Apparently, this solenoid produced the most uniform field; thus, it gave the most accurate measurements. This solenoid was used to conduct all subsequent tests.

Resistance in Coil

At low frequencies, the real part of the measured impedance Z' is dominated by the resistance in the solenoid coil R_{coil} . Fig. 10(d) shows that failure to account for the coil resistance in imaginary permeability calculations results in a characteristic linear increase in imaginary permeability with decreasing frequency when data are plotted on a log-log scale, as predicted by (12). Subsequent imaginary permeability data are presented with the effect of the resistance in coil removed ($R_{\text{coil}} \approx 0.817 \Omega$).

Residual Parameters

Data shown in Fig. 10 indicate that a resonant trend develops at frequencies greater than $\approx 10^5$ Hz. This resonance is

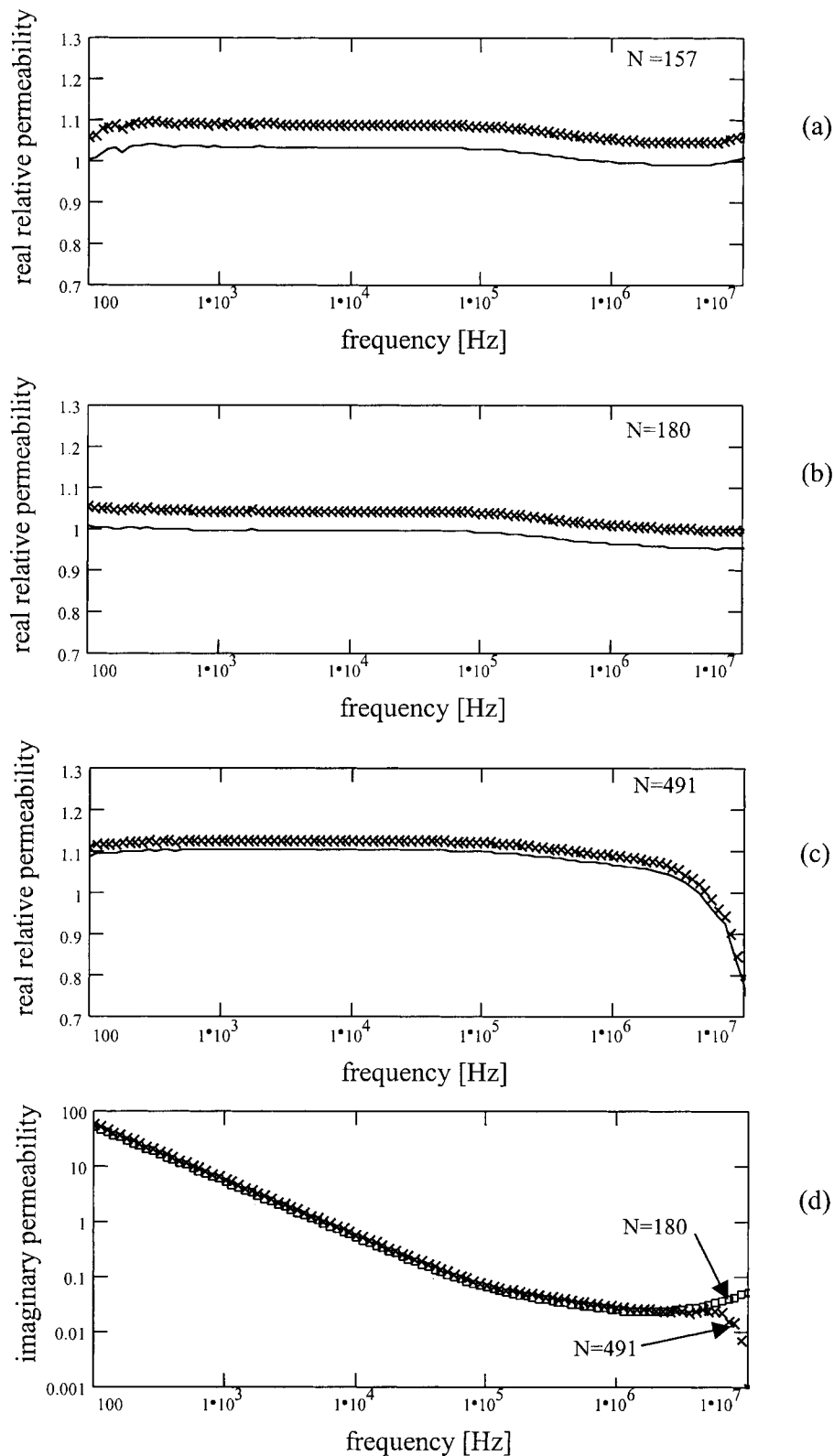


FIG. 10. Relative Magnetic Permeability Measurements of Air Using Different Solenoids. Lines Denote Values Corrected for Geometry [Eqs. (12) and (13)]

due to the interaction between the device under test and the electronic circuitry. As this connection is often unstable, no correction is implemented, and data above $\approx 10^5$ Hz are disregarded.

Incomplete Field Coverage

The solenoid creates a magnetic field inside and outside the solenoid; however, the specimen only fills the inside. Two tests

were conducted to evaluate this effect on the extreme condition of 100% iron filings: (1) Iron filings only inside the solenoid; and (2) iron filings inside and completely surrounding the solenoid. Results are shown in Fig. 11. Slightly lower values in real and imaginary magnetic permeabilities are measured when the specimen is only inside the solenoid as compared to the case in which the specimen surrounds the solenoid. For this solenoid and specimen, errors in real and

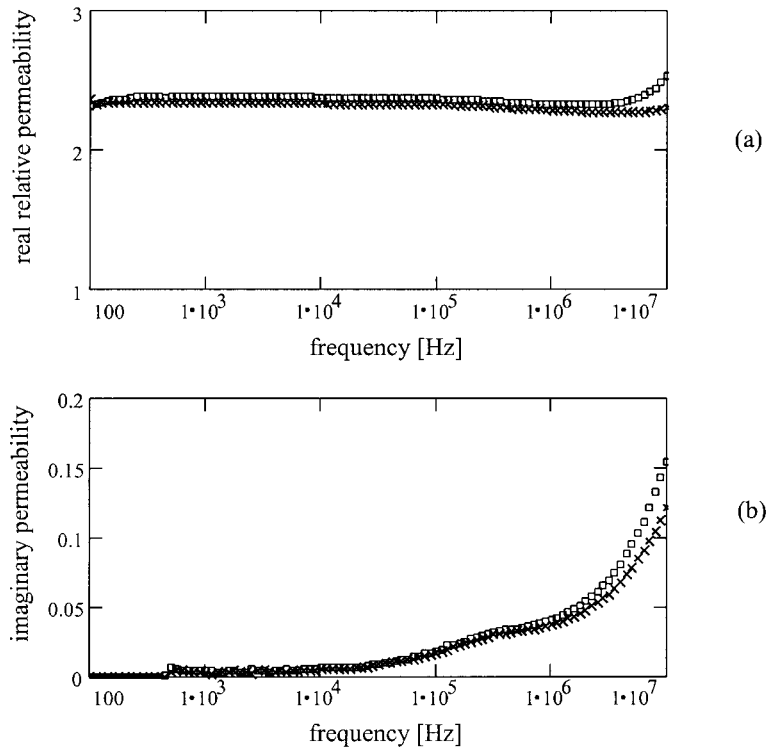


FIG. 11. Measured Magnetic Permeability of Iron Filings. Specimen Only within Solenoid (x) and Surrounding Solenoid (□): (a) Real Relative Magnetic Permeability; (b) Imaginary Relative Magnetic Permeability. Solenoid Characteristics: $l = 7.4$ cm, $A = 0.449$ cm², and $N = 180$

imaginary permeabilities are less than 2 and 7%, respectively, when only the solenoid is filled (within the reliable frequency range less than $\approx 10^5$ Hz).

EXPERIMENTAL STUDY 1: CONCENTRATION OF DISSEMINATED FERROMAGNETIC INCLUSIONS

The goals of these measurements are to look at the effect of ferromagnetic inclusions on the magnetic behavior of a non-ferromagnetic soil and to develop a simple relationship between the amount of ferromagnetic inclusions and magnetic permeability. Magnetic permeability measurements were performed on specimens of air-dried kaolinite (<0.075-mm diameter) with different percentages of fine iron filings (≈ 40 mesh, Fisher Scientific). The volume fraction of ferromagnetic inclusions ranged from 0 to 0.31; the characteristics of the specimens are presented in Table 5. Variations in the real and imaginary relative magnetic permeabilities of these mixtures were determined following the procedure described previously. Note that the presence of moisture does not affect these measurements.

Fig. 12 presents the real and imaginary permittivity data of the various mixtures. The real relative magnetic permeability remains constant over the frequency range of 100 to 10^5 Hz for all specimens and increases as the iron content increases. The imaginary relative permeability is fairly constant at low frequencies and then increases with increasing frequencies. Table 5 summarizes the real and imaginary permeability measurements at 10 kHz. The calibration curves with air presented in Fig. 10 show similar variations in real and imaginary values with frequency as the measured data in Fig. 12, particularly at frequencies $>10^5$ Hz. These similarities confirm that the decrease in real permeability and the change in imaginary permeability at frequencies $>10^5$ Hz are a result of cell-device coupling.

The low frequency real relative magnetic permeability of the mixtures is plotted versus the volume fraction of ferro-

TABLE 5. Permeability Measurements for Kaolinite Specimens with Different Concentrations of Iron Filings (Estimated Error $\pm 0.3\%$)

Percent iron filings (by weight) (1)	Volume fraction of iron v_2 (2)	μ'_{rel} ($f = 10$ kHz) (3)	μ''_{rel} ($f = 10$ kHz) (4)
0	0.000	1.001	0.0006
1	0.001	1.008	0.001
10	0.011	1.053	0.001
25	0.032	1.158	0.003
50	0.091	1.454	0.006
75	0.176	1.946	0.006
100	0.313	2.924	0.013

magnetic inclusions v_2 in Fig. 13. A second degree polynomial is fitted to the data

$$\mu'_{rel} = 1 + 4 \cdot v_2 + 7 \cdot v_2^2 \quad (15)$$

or in terms of the real susceptibility

$$\chi' = (\mu'_{rel} - 1) = 4 \cdot v_2 + 7 \cdot v_2^2 \quad (16)$$

Eq. (15) shows that for low volume fractions of ferromagnetic inclusions, the real relative permeability increases linearly; however, as v_2 increases, interactions between particles dominate the behavior, and the permeability increases parabolically. Fig. 13 also compares the measured data with the Wagner (Gokturk et al. 1993), Poisson (Doyle 1978), and Doyle (1978) noninteracting models. These models give similar values for volume fraction of inclusions $v_2 < 0.2$; for $v_2 > 0.25$, the Doyle model presents the highest permeability values. The underprediction of the measured data by these models and the nonlinearity of the measured data concur to indicate particle-

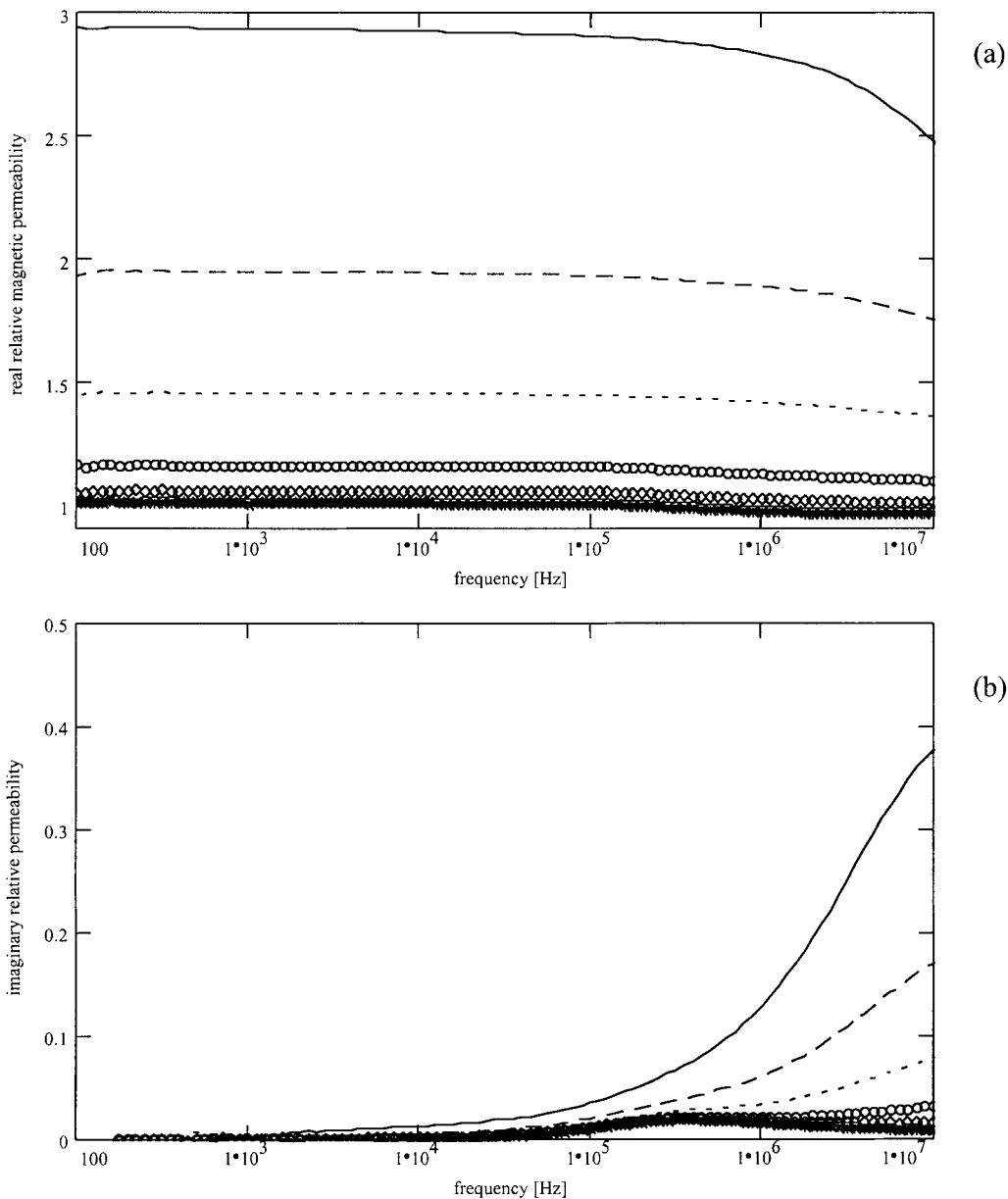


FIG. 12. Magnetic Permeability Measurements for Kaolinite-Iron Filing Mixtures with Different Weight Percentage of Iron Filings: (a) Real Relative Magnetic Permeability; (b) Imaginary Relative Magnetic Permeability. (— = 100% Fe; --- = 75% Fe; ··· = 50% Fe; ○ = 25% Fe; ◇ = 10% Fe; □ = 1% Fe; + = Kaolinite; and × = Air)

particle interactions even at low concentrations, for v_2 greater than ≈ 0.05 .

EXPERIMENTAL STUDY 2: SPATIAL DISTRIBUTION OF FERROMAGNETIC INCLUSIONS

Because interactions between ferromagnetic inclusions in a nonferromagnetic host medium affect the overall magnetic permeability of the mixture, the spatial distribution of inclusions must also impact the magnetic properties. The purpose of this second study is to identify variations in real and imaginary magnetic permeabilities caused by different spatial distributions of the same mass and volume fraction of ferromagnetic inclusions. Measurements were performed on air-dried kaolinite specimens containing metal rods (0.9-mm diameter) of various lengths and spatial arrangements, as shown in Fig. 14. The volume fraction of ferromagnetic inclusions in Specimens c–g is 0.014.

Fig. 15 presents the real and imaginary permeabilities for the various specimens. Clear relaxations are observed

within the reliable frequency range ($f < 10^5$ Hz). Table 6 summarizes these results. Difficulties in determining the relaxation frequency of the randomly oriented ferromagnetic inclusions (Specimen g) develop because the effect of residual equipment parameters begins to manifest at these frequencies.

The low frequency real and imaginary permeability values increase and the relaxation frequency decreases as the size of the inclusions increases. Possible underlying mechanisms include

- Magnetization of ferromagnetic inclusions by wall bowing (single relaxation).
- Enhanced interactions between domains within the longer rods or nearby rods (increase in real magnetic permeability with increasing size of ferromagnetic rods).
- Higher eddy current losses develop as the size of the continuous metal phase increases (decreasing relaxation frequency with increasing inclusions size and increasing imaginary permeability).

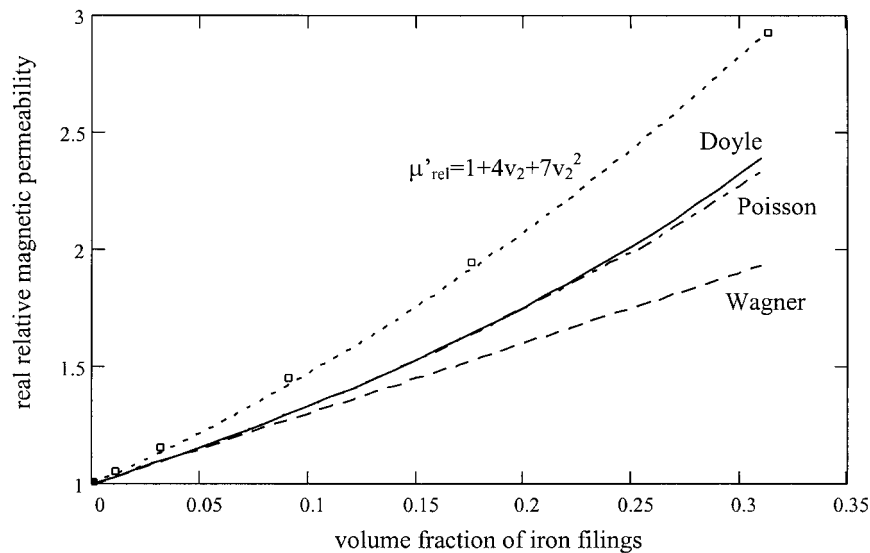


FIG. 13. Characterization of Kaolinite-Iron Filing Mixtures. Real Relative Magnetic Permeability Data Were Obtained at 10 kHz. Three Mixture Models Are Shown (Note: 100% Iron Filings by Weight Corresponds to Volume Fraction of 0.31)

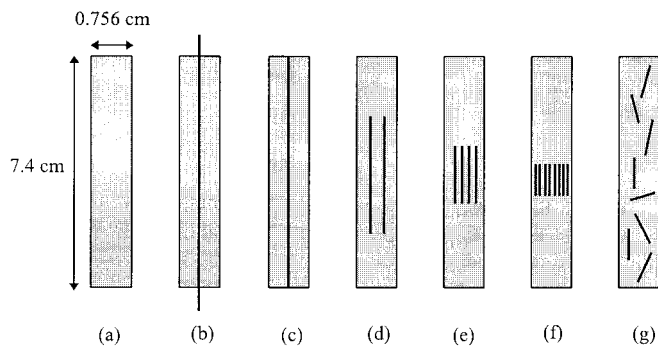


FIG. 14. Spatial Distribution of Ferromagnetic Inclusions (Thin Metal Rods, 0.9-mm Diameter) in Kaolinite. Specimens 3–7 Have Same Total Volume of Ferromagnetic Inclusions (Volume Fraction = 0.014). Specimen a Consists of Kaolin without Ferromagnetic Inclusions. Specimen b Is Prepared to Verify Low Impact of Geometric Effects

IMPLICATIONS OF FERROMAGNETIC MATERIALS ON PERMITTIVITY MEASUREMENTS

The addition of ferromagnetic inclusions to a nonconducting host medium has two effects on the inferred dielectric permittivity. The first effect is physical, and it is caused by the conductive nature of the inclusions. (Note that all ferromagnetic materials are not conductive.) The second effect is due to improper data interpretation.

Physical Effect of Conductive Inclusions on Mixture Permittivity

The placement of a spherical conducting particle in an electric field produces charge displacement toward the surface of the particle, thereby polarizing the particle (the electric field inside the particle is zero). Thus, the presence of nonpercolating metallic particles in a low permittivity medium significantly increases the overall dielectric permittivity of the mixture (Gokturk et al. 1993).

Table 7 presents selected mixture models that describe the high frequency limit permittivity κ''_{inf} of mixtures of conducting inclusions in a dielectric host medium. All models have been simplified by assuming that the permittivity of the inclusions is much greater than the permittivity of the host medium ($\kappa'_2 \gg \kappa'_1$). Fig. 16 shows the computed mixture permittivity

as a function of the volume fraction of conducting inclusions for the different models. All models give similar permittivity values when the volume fraction of inclusions is less than about 0.1.

Effect of Ferromagnetism on Interpreted Permittivity Values

Most laboratory and field studies of geomaterials using electromagnetic waves are interpreted assuming that the material is nonferromagnetic. However, if the medium has $\mu^* \neq \mu_0$, inferred permittivities will be incorrect. This error is analyzed in the context of the wave equation for electromagnetic phenomena, which follows from Maxwell's equations. If a solution of the form

$$E = E_0 e^{(j\omega t - \gamma^* x)} \quad (17)$$

is adopted and substituted into the wave equation, a complex "propagation constant," γ^* emerges

$$\gamma^* = \frac{2\pi f}{c_0} \sqrt{-(\mu'_{rel} - j \cdot \mu''_{rel})(\kappa' - j \cdot \kappa''_{eff})} \quad (m^{-1}) \quad (18)$$

where c_0 = velocity of electromagnetic waves in free space ($c_0 = 3 \times 10^8$ m/s); f = frequency (Hz); and κ' = real part of the relative permittivity. The effective imaginary relative permittivity κ''_{eff} includes conduction and polarization losses

$$\kappa''_{eff} = \kappa''_{pol} + \frac{\sigma}{\omega \epsilon_0} \quad (19)$$

The presence of moisture affects conduction and polarization (i.e., σ , κ'' , and κ'). Therefore, the effect of moisture is explicitly considered in this formulation. If nonferromagnetic materials are assumed ($\mu'_{rel} = 1$ and $\mu''_{rel} = 0$)

$$\gamma^* = \frac{2\pi f}{c_0} \sqrt{-(\kappa' - j \cdot \kappa''_{eff})} \quad (m^{-1}) \quad (20)$$

Thus, if (20) is used to infer parameters for a medium with $\mu^* \neq \mu_0$ [(18)], the computed permittivity becomes [setting (18) equal to (20)]

$$\kappa'_{(inferred)} = \mu'_{rel} \kappa' - \kappa''_{eff} \mu''_{rel} \quad (21)$$

$$\kappa''_{eff(inferred)} = \mu'_{rel} \kappa''_{eff} + \kappa' \mu''_{rel} \quad (22)$$

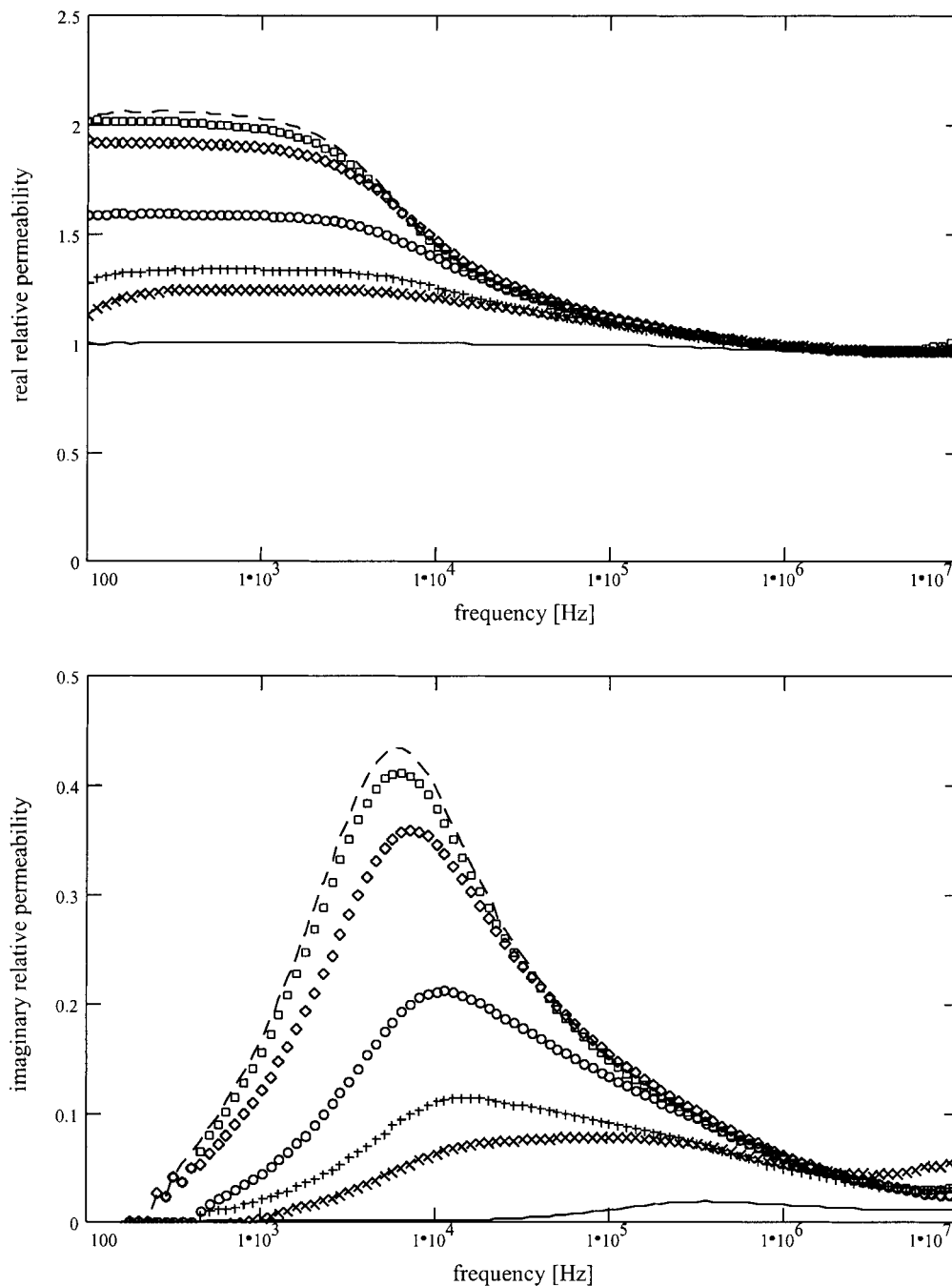


FIG. 15. Magnetic Permeability Measurements of Kaolinite Containing Ferromagnetic Inclusions with Different Spatial Distributions (Refer to Fig. 14). Specimens Are Denoted as Follows: a, —; b, ---; c, □; d, ◇; e, ○; f, +; and g, ×

TABLE 6. Permeability Measurements for Kaolinite Specimens with Different Sizes and Spatial Distributions of Ferromagnetic Inclusions

Number of inclusions (1)	Length of inclusions (cm) (2)	Spatial distribution ^a (3)	μ'_{rel} ($f = 1$ kHz) (4)	Relaxation frequency (kHz) (5)	μ''_{rel} ($f = 10$ kHz) (6)
0	—	(a)	1	—	0.002
1	10.5	(b)	2.03	5.6	0.398
1	7.4	(c)	1.98	6.3	0.380
2	3.7	(d)	1.89	7.1	0.347
4	1.85	(e)	1.58	11.2	0.211
8	0.92	(f)	1.24	14.1	0.063
8	0.92	(g)	1.34	≈15.8	0.110

^aSee Fig. 14 for schematic drawings of spatial distributions of ferromagnetic inclusions.

If the imaginary permeability is negligible, $\mu''_{rel} = 0$, the true permittivity values can be obtained from the inferred values as

$$\kappa'_{true} = \frac{\kappa'_{(inferred)}}{\mu'_{rel}} \quad (23)$$

$$\kappa''_{true} = \frac{\kappa''_{(inferred)}}{\mu'_{rel}} \quad (24)$$

This result shows that failure to account for the magnetic permeability of a mixture containing ferromagnetic inclusions results in a higher measured permittivity than the true mixture permittivity. The permittivity data must be corrected using magnetic permeability measurements conducted at the same frequencies as the permittivity measurements, as both permittivity and permeability are functions of frequency.

TABLE 7. High Frequency Permittivity Models for Conductor-Dielectric Mixtures

Model (1)	Equation (2)	Comments (3)
Rayleigh's octupole formula ^a	$\kappa'_{\text{mix}} = \kappa'_1 \left(1 + \frac{3v_2}{1 - v_2 - 1.65v_2^{10/3}} \right)$	Spherical particles; $\kappa'_2 \gg \kappa'_1$
Wagner ^{a,b}	$\kappa'_{\text{mix}} = \kappa'_1(1 + 3v_2)$	Spherical particles; $v_2 < 0.2$; $\kappa'_2 \gg \kappa'_1$
Bruggeman ^a	$\kappa'_{\text{mix}} = \kappa'_1 \frac{1}{(1 - v_2)^3}$	Spherical particles; $\kappa'_2 \gg \kappa'_1$
Bottcher ^{a,b}	$\kappa'_{\text{mix}} = \kappa'_1 \frac{1}{1 - 3v_2}$	Spherical particles; $v_2 < 1/3$; $\kappa'_2 \gg \kappa'_1$
deLoor ^{1,b}	$\kappa'_{\text{mix}} = \kappa'_1 \frac{1 + v_2}{1 - 2v_2}$	Spherical particles; $v_2 < 0.2$; $\kappa'_2 \gg \kappa'_1$
van Beek ^{a,b}	$\kappa'_{\text{mix}} = \kappa'_1 \frac{1 - v_2}{1 - 4v_2}$	Spherical particles; $v_2 < 0.2$; $\kappa'_2 \gg \kappa'_1$
Clausius-Mossotti ^c	$\kappa'_{\text{mix}} = \kappa'_1 \frac{1 + 2v_2}{1 - v_2}$	Conducting spheres in cubic array; $\kappa'_2 \gg \kappa'_1$
Doyle ^c	$\kappa'_{\text{mix}} = \kappa'_1 \frac{[1 + 2v_2 - 1.305v_2^{10/3}]}{[1 - v_2 - 1.305v_2^{10/3}]}$	Conducting spheres in simple cubic array; $v_2 < 0.67$; $\kappa'_2 \gg \kappa'_1$

Note: κ'_{mix} , κ'_1 , and κ'_2 = permittivity of mixture, host medium, and conducting inclusions, respectively; and v_2 = volume fraction of inclusions.
^aLal and Parshad (1973).
^bvan Beek (1967).
^cDoyle (1978).

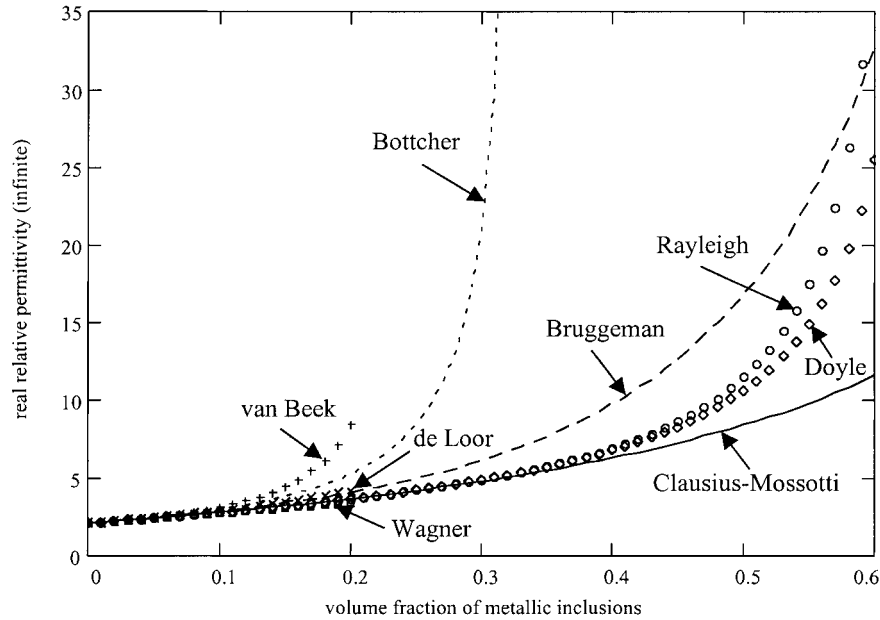


FIG. 16. Real Relative Dielectric Permittivity Models for Conductive Inclusions in Dielectric Host Medium (Infinite Permittivity)

ENGINEERING IMPLICATIONS

The implementation of geophysical techniques (e.g., ground-penetrating radar) based on electromagnetism is restricted by the trade-off between the desired resolution and the achievable skin depth. Spatial resolution can be estimated from the wavelength λ . Recognizing that γ^* plays the role of a complex wave number in (17), the wavelength can be computed from (18)

$$\lambda = \frac{2\pi}{\text{Im}[\gamma^*]} = \frac{c_0}{f} \cdot \frac{1}{\text{Im}[\sqrt{-(\mu'_{rel} - j \cdot \mu''_{rel})(\kappa' - j \cdot \kappa''_{eff})}]} \quad (25)$$

where $\text{Im}[\]$ indicates the imaginary part of the quantity in brackets. In the case of zero polarization and ohmic losses, $\kappa''_{eff} \approx 0$, and nonferromagnetic materials, $\mu^* = \mu_0$, (25) reduces to $\lambda = c_0/f(\kappa')^{1/2}$. On the other hand, the depth of pen-

etration into the medium can be estimated by computing the "skin depth," S_d (m)

$$S_d = \frac{1}{\alpha} = \frac{1}{\text{Re}[\gamma^*]} = \frac{c_0}{2\pi f} \cdot \frac{1}{\text{Re}[\sqrt{(\mu'_{rel} - j \cdot \mu''_{rel})(-\kappa' + j \cdot \kappa''_{eff})}]} \quad (26)$$

where α = attenuation; and $\text{Re}[\]$ indicates the real part of the quantity in brackets.

Wave velocity is also affected by the presence of ferromagnetic materials

$$v = \lambda \cdot f = c_0 \cdot \frac{1}{\text{Im}[\sqrt{-(\mu'_{rel} - j \cdot \mu''_{rel})(\kappa' - j \cdot \kappa''_{eff})}]} \quad (\text{m/s}) \quad (27)$$

Finally, ferromagnetic behavior also changes the amplitude and phase of reflected signals, such as in ground-penetrating radar applications. The reflection coefficient is

$$refl^* = \frac{z_2^* - z_1^*}{z_2^* + z_1^*} = \frac{1 - z_1^*/z_2^*}{1 + z_1^*/z_2^*} \quad (28)$$

where z_1^* and z_2^* = specific impedance of the first medium and the reflecting medium, respectively, and are computed as

$$z^* = j \frac{\omega}{\gamma^*} \mu^* \quad (29)$$

Consider a medium with $\mu'_{rel} = 1.25$, $\mu''_{rel} = 0$, $\kappa' = 60$, $\kappa''_{pot} = 0$, and $\sigma = 0.1$ S/m, which is illuminated by an electromagnetic wave at a frequency of 50 MHz. The resulting wave velocity is 3.33×10^7 m/s (for $\mu' = 0$, the velocity is 3.72×10^7 m/s), and the skin depth is 0.38 m (for $\mu' = 0$, $S_d = 0.43$ m). The inferred real permittivity is $\kappa'_{inferred} = 75$ and the inferred conductivity is $\sigma_{inferred} = 0.125$ S/M. Should the real permittivity be used to estimate moisture content or void ratio (in a saturated medium), the resulting error would be significant.

SUMMARY

The magnetic properties of matter reflect the presence of moving charges. Some materials possess permanent magnetic moments and are classified as paramagnetic or ferromagnetic. Materials without permanent magnetic moments are diamagnetic. The magnetic permeability/susceptibility can be measured using various available methods including force-based systems, change-in-flux techniques, and transmission/reflection methods.

Different low frequency magnetization mechanisms occur in ferromagnetic materials as the applied magnetic field increases. Wall bowing takes place at low field intensity, and as the field intensity increases, wall displacement and then the rotation of domain spins manifest.

Magnetic permeability is a function of the frequency of the applied field. Low frequency dispersions in ferromagnetic materials occur at kilohertz and megahertz frequencies as a result of movement of domain walls. High frequency electron spin resonance manifests at gigahertz frequencies. Given that magnetic permeability is a frequency dependent property, quasi-DC and low frequency measurements render permeability values that may not be applicable to high frequency field applications such as ground penetrating radar and time-domain reflectometry. In general, the equations presented here are applicable for parameters measured at the same frequency, with no restriction on the frequency range.

An empirical relationship was identified between magnetic permeability and the amount of disseminated ferromagnetic particles present in a nonferromagnetic soil. This equation is linear at low volume fractions where there are no particle-to-particle interactions and becomes a second-order polynomial as iron content increases, thus capturing interaction effects. Further experimental studies show that the size, proximity, and spatial distribution of ferromagnetic inclusions significantly affect the permeability of the medium.

Although the nonferromagnetic assumption is frequently invoked in laboratory and field studies, neglecting the presence of ferromagnetic materials results in a higher permittivity than the true mixture permittivity. The presence of nonpercolating, conductive materials also acts to increase the permittivity of the mixture.

The propagation of electromagnetic waves in geomaterials is affected by the presence of ferromagnetic inclusions. Ferromagnetic materials impact wavelength, skin depth, wave velocity, and the reflection coefficient. Therefore, failure to consider the presence of ferromagnetic materials in the interpretation of data obtained using various in situ and laboratory electromagnetic measurement techniques can result in erroneous interpretations.

ACKNOWLEDGMENTS

This study is part of a research program on wave-based characterization of geomaterials, which is supported by the National Science Foundation and the Georgia mining industry.

APPENDIX. REFERENCES

- Adler, E., Reppel, G. W., Rodewald, W., and Warlimont, H. (1989). "Matching P/M and the physics of magnetic materials." *Int. J. Powder Metallurgy*, 25(4), 319–335.
- Baker-Jarvis, J., Janezic, M. D., Grosvenor, J. H., and Geyer, R. G. (1993). "Transmission/reflection and short-circuit line methods for measuring permittivity and permeability." *NIST Tech. Note 1355-R*, Boulder, Colo.
- Bleaney, B. I., and Bleaney, B. (1976). *Electricity and magnetism*, 3rd Ed., Oxford University Press, New York.
- Bozorth, R. M. (1951). *Ferromagnetism*, D. Van Nostrand Company, Inc., New York.
- Carmichael, R. S. (1989). *CRC practical handbook of physical properties of rocks and minerals*. CRC, Boca Raton, Fla.
- Daniels, J. J., and Roberts, R. L. (1994). "Ground penetrating radar for geotechnical applications." *Geophysical characterization of sites, IS-SMFE Tech. Committee No. 10*, R. Woods, ed., Oxford and IBS Publishing Co. Pvt. Ltd., New Delhi, 1–13.
- Doyle, W. T. (1978). "The Clausius-Mossotti problem for cubic arrays of spheres." *J. Appl. Phys.*, 49(2), 795–797.
- Edwards, R. N., and Nabighian, M. N. (1991). "The magnetometric resistivity method." *Electromagnetic methods in applied geophysics: Volume 2, Application, Parts A and B, Investigations in Geophysics No. 3*, M. Nabighian, ed., Society of Exploration Geophysics, Tulsa, Okla., 47–104.
- Gelinas, C., Chagnon, F., Pelletier, S., and Lefebvre, L. P. (1997). "Iron-resin composites for high frequency AC magnetic applications." *Advances in Powder Metallurgy and Particulate Mat., Proc., 1997 Int. Conf. on Powder Metallurgy and Particulate Mat.*, Vol. 1, Part 1, Compiled by R. A. McKotch and R. Webb, Metal Power Industries Federation, Princeton, N.J., 1-37–1-45.
- Gokturk, H. S., Fiske, T. J., and Kalyon, D. M. (1993). "Electric and magnetic properties of a thermoplastic elastomer incorporated with ferromagnetic powders." *IEEE Trans. on Magnetics*, 29(6), 4170–4176.
- Halliday, D., and Resnick, R. (1988). *Fundamentals of physics*, 3rd Ed., Wiley, New York.
- Hashin, Z., and Shtrikman, S. (1962). "A variational approach to the theory of the effective magnetic permeability of multiphase materials." *J. Appl. Phys.*, 33(10), 3125–3131.
- Hatfield, W. E. (1987). "Chapter 4—Magnetic measurements." *Solid-state chemistry techniques*, A. K. Cheetham and P. Day, eds., Oxford University Press, New York.
- Klein, K., and Santamarina, J. C. (1997). "Methods for broad-band dielectric permittivity measurements (soil-water mixtures, 5 Hz to 1.3 GHz)." *Geotech. Testing J.* 20(2), 168–178.
- Lal, K., and Parshad, R. (1973). "Permittivity of conductor-dielectric heterogeneous mixtures." *J. Phys. D: Appl. Phys.*, 6, 1788–1792.
- Landau, L. D., Lifshitz, E. M., and Pitaevskii, L. P. (1984). *Electrodynamics of continuous media*, 2nd Ed., Vol. 8, Pergamon, New York.
- Marshall, D. J., and Madden, T. R. (1959). "Induced polarization, a study of its causes." *Geophysics*, 24(4), 790–816.
- Mulay, L. N. (1972). "Chapter VII—Techniques for measuring magnetic susceptibility." *Techniques of chemistry, Volume 1—Physical methods of chemistry: Part IV Determination of mass, transport, and electrical-magnetic properties*, Weissberger and Rossiter, eds., Wiley-Interscience, New York, 431–553.
- Omar, M. A. (1975). *Elementary solid state physics*. Addison-Wesley, Reading, Mass.
- Schroeder, P. A., Pruett, R. J., and Hurst, V. J. (1998). "Effects of secondary iron phases on kaolinite ²⁷Al MAS NMR spectra." *Clays and Clay Minerals*, 46(4), 429–435.
- Topp, G. C., Davis, J. L., Bailey, W. G., and Zebchuk, W. D. (1984). "The measurement of soil water content using a portable TDR hand probe." *Can. J. Soil Sci.*, Ottawa, 64, 313–321.
- Valenzuela, R. (1994). *Magnetic ceramics*. University Press, Cambridge, U.K.
- van Beek, L. K. H. (1967). "Dielectric behaviour of heterogeneous systems." *Progress in dielectrics*, Vol. 7, Heywood Books, U.K.
- Ward, S. H. (1990). "Resistivity and induced polarization methods." *Geotechnical and environmental geophysics, Volume I: Review and tutorial, Investigations in Geophysics No. 5*, S. Ward, ed., Society of Exploration Geophysics, Tulsa, Okla., 147–189.
- Welsby, V. G. (1950). *The theory and design of inductance coils*. MacDonald and Co. (Publishers) Ltd., London.